

Article

# Microwave-Assisted Synthesis of N/TiO<sub>2</sub> Nanoparticles for Photocatalysis under Different Irradiation Spectra

Camilo Sanchez Tobon <sup>1,\*</sup>, Davor Ljubas <sup>1,\*</sup>, Vilko Mandić <sup>2</sup>, Ivana Panžić <sup>2</sup>, Gordana Matijašić <sup>2</sup> and Lidija Čurković <sup>1,\*</sup>

<sup>1</sup> Faculty of Mechanical Engineering and Naval Architecture, University of Zagreb, 10000 Zagreb, Croatia

<sup>2</sup> Faculty of Chemical Engineering and Technology, University of Zagreb, 10000 Zagreb, Croatia; vmandic@fkit.hr (V.M.); ipanzic@fkit.hr (I.P.); gmatijas@fkit.hr (G.M.)

\* Correspondence: camilo.sanchez.tobon@fsb.hr (C.S.T.); davor.ljubas@fsb.hr (D.L.); lidija.curkovic@fsb.hr (L.Č.)

**Abstract:** Nitrogen-doped TiO<sub>2</sub> (N/TiO<sub>2</sub>) photocatalyst nanoparticles were derived by the environmentally friendly and cost-effective microwave-assisted synthesis method. The samples were prepared at different reaction parameters (temperature and time) and precursor ratio (amount of nitrogen source; urea). The obtained materials were characterized by X-ray diffraction (XRD), photoelectron spectroscopy (XPS), Raman spectroscopy (RS), infrared spectroscopy (FTIR), diffuse reflectance spectroscopy (DRS), electron microscopy (SEM-EDS), and nitrogen adsorption/desorption isotherms. Two cycles of optimizations were conducted to determine the best reaction temperature and time, as well as N content. The phase composition for all N/TiO<sub>2</sub> nanomaterials was identified as photoactive anatase. The reaction temperature was found to be the most relevant parameter for the course of the structural evolution of the samples. The nitrogen content was the least relevant for the development of the particle morphology, but it was important for photocatalytic performance. The photocatalytic activity of N/TiO<sub>2</sub> nanoparticle aqueous suspensions was evaluated by the degradation of antibiotic ciprofloxacin (CIP) under different irradiation spectra: ultraviolet A light (UVA), simulated solar light, and visible light. As expected, all prepared samples demonstrated efficient CIP degradation. For all irradiation sources, increasing synthesis temperature and increasing nitrogen content further improved the degradation efficiencies.

**Keywords:** microwave-assisted synthesis; N/TiO<sub>2</sub>; ciprofloxacin; UVA; visible light; simulated solar light



**Citation:** Sanchez Tobon, C.; Ljubas, D.; Mandić, V.; Panžić, I.; Matijašić, G.; Čurković, L. Microwave-Assisted Synthesis of N/TiO<sub>2</sub> Nanoparticles for Photocatalysis under Different Irradiation Spectra. *Nanomaterials* **2022**, *12*, 1473. <https://doi.org/10.3390/nano12091473>

Academic Editor: Marianna Kemell

Received: 30 March 2022

Accepted: 22 April 2022

Published: 26 April 2022

**Publisher's Note:** MDPI stays neutral with regard to jurisdictional claims in published maps and institutional affiliations.



**Copyright:** © 2022 by the authors. Licensee MDPI, Basel, Switzerland. This article is an open access article distributed under the terms and conditions of the Creative Commons Attribution (CC BY) license (<https://creativecommons.org/licenses/by/4.0/>).

## 1. Introduction

Nowadays, owing to the fast-growing population and the development of industries, where thousands of chemical substances are produced, the risk of an unregulated release of harmful substances into the environment is significant. Among all kinds of pollutants that enter the water bodies every day, organic micropollutants (OMPs) have gained significant attention in the last 20 years due to their impact on the environment [1]. These OMPs, which are mainly pharmaceuticals, personal care products, disinfection by-products, and endocrine disruptors, have been found to be harmful to aquatic life because they are persistent, and some of them bioaccumulate over time, promoting the appearance of antibiotic-resistant bacteria [2–5]. Additionally, it has been shown that conventional wastewater treatment plants (WWTPs) have problems removing some OMPs, i.e., the conventional WWTPs do not prevent their entry into the environment [6]. Therefore, it is necessary to develop new treatment technologies that can be linked to the existing WWTPs to remove these OMPs efficiently.

Advanced oxidation processes (AOPs) have been considered as an excellent alternative for the removal of OMPs [7,8]. In general, AOPs, such as Fenton, electrochemical

oxidation, ozonation, photocatalysis, etc., rely on the generation of reactive oxygen species (ROS) such as hydroxyl radical to oxidize organic pollutants present in the water [9–11]. Among different AOPs, TiO<sub>2</sub> heterogeneous photocatalyst is actively studied because of its outstanding photocatalytic activity, low-cost, excellent chemical stability, and non-toxicity [12–14]. However, TiO<sub>2</sub> is photoactive only under ultraviolet (UV) light irradiation due to its high bandgap (3.2 eV), limiting its application under solar irradiation (4% UV, 48% visible). Moreover, the photogenerated electron-hole pair, that initiates the redox reactions, can quickly recombine, decreasing the photocatalytic activity [15–18]. Therefore, modification of the TiO<sub>2</sub> unit cell by means of doping can be a strategy to reduce the recombination rate and/or to redshift its optical response to the visible light range.

Metal doping, such as Pd, Pt, Au, etc., has shown improved photocatalytic activity in the visible range. However, the high metal costs and probability of metal leaching due to low thermal stability, which might represent a health risk, reduce its applicability [12,15,19]. Therefore, non-metal doping, such N, P, S, and C, seem to be more feasible and less expensive to enhance photoactivity under solar spectrum irradiation [20–22]. Among non-metal doping, nitrogen is widely studied due to its similarity in atomic radius with oxygen, making more probable the atomic substitution [23]. Nitrogen-doped TiO<sub>2</sub> has shown an interesting photoactive response under visible light, and this can be attributed to the formation of new energetic levels that reduce the energy bandgap [24]. Additionally, some studies suggest that nitrogen could favor the TiO<sub>2</sub> anatase phase formation, which is the most photoactive TiO<sub>2</sub> polymorph [25].

On the other hand, TiO<sub>2</sub> photoefficiency can be affected by its morphological, optical, and structural properties, which can be to an extent governed by the synthesis method [26,27]. Some of the common conventional synthesis strategies are the sol-gel method, chemical vapor deposition, hydrothermal, etc. The main drawbacks of these methods are the pricy resourcing and long synthesis time [28]. However, the microwave-assisted method first emerged as a non-conventional heating method and was soon recognized as an effective method due to the environmental friendliness, shorter synthesis time, and both homogeneous and selective distribution of heating on greater amounts of samples [29,30].

As a model waste substance, an aqueous solution of ciprofloxacin was used. Ciprofloxacin (CIP) is a fluoroquinolone antibiotic used for the treatment of a wide variety of infections [31–33], and it is one of the most often found OMPs in the effluents of wastewaters, surface waters, and drinking waters, with a concentration up to 6.5 mg/L [7]. Due to the lack of its removal by biological systems and due to inaccurate information about its toxicity and bioaccumulation, it was included in the second EU watch list of substances for union-wide monitoring in the field of water policy (Decision (EU) 2018/840 of 5 June 2018) and is still under monitoring in the third EU watch list (Decision (EU) 2020/1161 of 4 August 2020) [34,35]. CIP removal from the wastewaters was attempted by adsorption and biological membrane bioreactors, but the removal efficiencies were substandard [36,37].

Therefore, this study focuses on the synthesis of N/TiO<sub>2</sub> photocatalyst using the non-conventional microwave-assisted method, evaluating the role of the temperature, reaction time, and nitrogen content on the structural and morphological properties of the synthesized materials, as well as on the photocatalytic activity under different radiation sources.

## 2. Materials and Methods

### 2.1. Materials

Titanium (IV) isopropoxide (TTIP, 97%, Sigma-Aldrich, St. Louis, MO, USA), acetylacetone ( $\geq 99\%$ , Honeywell, Charlotte, NC, USA), ethanol absolute (p.a., Grammol, Zagreb, Croatia), urea (99.05%, Sigma-Aldrich, St. Louis, MO, USA), Ciprofloxacin (CIP, 98%, Acros Organics, Waltham, MA, USA), and TiO<sub>2</sub> P-25 (cca. 80% anatase, 20% rutile, Degussa-Hüls Co., Frankfurt, Germany) were used as received without further purification. Deionized water was used throughout the experiments. For the investigation of photocatalytic degradation, a solution of antibiotic ciprofloxacin in deionized water of ultrapure quality (with

an electrical conductivity of 0.055  $\mu\text{S}/\text{cm}$  at 25 °C, produced with a model GenPure (TKA Co., Niederelbert, Germany) was used.

## 2.2. Microwave-Assisted Synthesis Parameters

For determining the microwave oven parameters in the N/TiO<sub>2</sub> synthesis, the sol-gel method was combined with the microwave-assisted method, using chemical reagents and ratios as described by Thapa et al. [38]. Briefly, TTIP was mixed with acetylacetonone (AcAc). Then, ethanol (EtOH) was added while stirring at room temperature. These reagents were mixed at molar ratio of TTIP:AcAc:EtOH = 0.014:0.039:1.37, and subsequently labeled as solution A. On the other hand, urea (N/Ti molar ratio equal 2) was dissolved in 20 mL deionized water and labeled as solution B. Solutions A and B were added dropwise to 80 mL of deionized water under continuous stirring at room temperature. The final solution was stirred for 1 h at room temperature. Then, the solution was transferred to four Teflon vessels in the microwave (MW) oven (Microwave Reaction System SOLV, Multiwave PRO, Anton-Paar GmbH, Graz, Austria) for thermal treatment at specific temperature and time. Inner pressure and temperature were monitored during the synthesis process. The synthesized material was washed several times with ethanol and water, centrifuged, and dried at 65 °C overnight. The chemical molar ratio of reagents was not evaluated. Instead, two different temperatures (150 °C and 200 °C) and three reaction times (10, 20, and 30 min) were considered as critical parameters for the microwave-assisted method. The obtained materials were labeled as N/TiO<sub>2</sub> T\_t, where T and t are the temperatures and time, respectively, used for the thermal treatment in the MW oven (Table 1).

**Table 1.** Material labeling and evaluated parameters.

Material Labeling	Parameter	Section
N/TiO <sub>2</sub> 150_10 N/TiO <sub>2</sub> 200_10 N/TiO <sub>2</sub> 200_20 N/TiO <sub>2</sub> 200_30	Temperature (from 150 to 200 °C) and time (from 10 to 30 min)	Microwave-assisted synthesis parameters (Section 2.2)
N/TiO <sub>2</sub> 0 N/TiO <sub>2</sub> 1 N/TiO <sub>2</sub> 2 N/TiO <sub>2</sub> 4 N/TiO <sub>2</sub> 12 N/TiO <sub>2</sub> 24	Nitrogen content (from 0 to 24 N/Ti molar ratio)	N/TiO <sub>2</sub> microwave-assisted synthesis parameters (Section 2.3)

## 2.3. N/TiO<sub>2</sub> Microwave-Assisted Synthesis

A similar procedure as described above was used to determine the effect of nitrogen in N/TiO<sub>2</sub> synthesis. However, the N/Ti molar ratio was varied (0, 1, 2, 4, 12, and 24) to evaluate the effect of nitrogen in the photocatalytic and morphological properties. Therefore, different amounts of urea were dissolved in 20 mL of deionized water and labeled as a solution B, (explained in the previous section). The other reagents were kept at the same molar ratio. Only one temperature and reaction time were used in the MW oven, based on the optimal parameters identified above (200 °C and 10 min). The obtained materials were labeled as N/TiO<sub>2</sub> x, where x represents the N/Ti molar ratio used (Table 1). Commercial TiO<sub>2</sub> Degussa P25 was used as a benchmark material for comparison purposes regarding morphological and photocatalytic properties.

## 2.4. Photocatalysts Characterization

For the XRD analysis, a Shimadzu XRD6000 (Shimadzu Corporation, Kyoto, Japan) X-ray diffractometer with CuK $\alpha$  radiation was used. The fixed step scans were collected in the 2 $\theta$  range 20–60° with steps of 0.02° 2 $\theta$  and counting time 0.6 s under accelerating voltage of 40 kV and current of 30 mA.

The BET surface area, pore volumes, and pore size distribution were estimated from nitrogen adsorption and desorption isotherm data using an ASAP 2000 apparatus (Micromeritics Corporation, Norcross, GA, USA). Prior to the analysis, the sample was degassed (6.6 Pa) at 150 °C to remove any physically adsorbed species. The pore size distribution of the sample was determined by the Barret–Joyner–Halenda model from the data of the adsorption and desorption branch of the nitrogen isotherms.

FTIR spectra were recorded on a Shimadzu IRSpirit (Shimadzu, Kyoto, Japan) in the range of 400–4000  $\text{cm}^{-1}$ .

Scanning electron microscopy (SEM) of the materials was performed using a Tescan Vega Easyprobe 3 device (Tescan, Brno, Czech Republic). Energy dispersive spectroscopy (EDS) spectra were recorded with a Bruker XFlash 6130 detector (Bruker, Billerica, MA, USA) at a working distance of 10 mm under accelerating voltage of 20 keV on uncoated samples glued to the stage using carbon two-side adhesive tape. EDS mapping was performed for Ti, O, and N.

Raman measurements were performed by confocal micro-Raman spectroscopy using a T64000 (Horiba Jobin Yvone, Kyoto, Japan) equipped with a solid-state laser with a wavelength of 532.5 nm and a 50 $\times$  magnification large working distance objective in the range of 90–2000  $\text{cm}^{-1}$ . Laser power at the sample was optimized to avoid heating and possible phase transition of  $\text{TiO}_2$  during measurement.

DRS measurements were performed on an Ocean Insight QE Pro High-Performance Spectrometer (Ocean Insight, Orlando, FL, USA) equipped with an integrating sphere for reflectance and a DH 2000 deuterium-halogen source in the range 250–950 nm with a resolution of 1 nm and integration time of 10 s.

The chemical composition and bonding were characterized by XPS in a SPECS XPS spectrometer equipped with a Phoibos MCD 100 electron analyzer (SPECS, Berlin, Germany) and a monochromatized source of  $\text{Al K}\alpha$  X-rays of 1486.74 eV. The typical pressure in the UHV chamber during analysis was in the  $10^{-7}$  Pa range. For the electron pass energy of the hemispherical electron energy analyzer of 10 eV was used in the present study, and the overall energy resolution was around 0.8 eV. All spectra were calibrated by the position of C 1s peak fixed at the binding energy of 284.5 eV. The XPS spectra were deconvoluted into several sets of mixed Gaussian–Lorentzian functions with Shirley background subtraction.

### 2.5. Photocatalytic Activity Evaluation

The photocatalytic activity evaluation was performed through the degradation of ciprofloxacin, using three different radiation sources: (I) ultraviolet A (UVA) lamp, model UVAHAND LED (Dr. Hönle AG, UV-Technologie, Gilching, Germany) (peak on 365 nm, 70 W), (II) solar light simulator (SLS), model SOL500 (Dr. Hönle AG, UV-Technologie, Gilching, Germany) (430 W), and (III) warm visible light lamp, model OSRAM Endura Flood 50 W WT, (Ledvance GmbH, Osram, Munich, Germany) (peaks on 450 nm and 600 nm, 50 W). In each experiment, 25 mg of the photocatalyst was dispersed in 100 mL of CIP solution (10 mg/L) and irradiated from above with lamps 20 cm away from the reactor. First, the suspension was stirred for 30 min in the dark to ensure adsorption-desorption equilibrium, which was determined previously by adsorption test. Then, the lamp was turned on and irradiated the suspension for 2 h. Samples were taken from the reactor at intervals of 0, 5, 10, 20, 30, 45, 60, 90, and 120 min, filtered using a 0.45  $\mu\text{m}$  mixed cellulose ester membrane filter, and analyzed with a UV-Vis spectrophotometer (HEWLETT PACKARD, Model HP 8430, Palo Alto, CA, USA) at 273 nm (maximum absorption peak of CIP). During the whole experiment, the temperature was kept at 25 °C by a thermostatic bath. All radiation spectra of the used lamps and UV-VIS absorbance of the 10 mg/L solutions of the CIP in water are given in Figure S1.

### 3. Results & Discussion

#### 3.1. Characterization of N/TiO<sub>2</sub> for Optimization of the Reaction Time and Temperature

To optimize the sample preparation in terms of the reaction temperature and time, the N/TiO<sub>2</sub> samples with constant N ratio were subjected to broad structural, microstructural, and spectroscopic characterization. For prepared N/TiO<sub>2</sub> materials, the nitrogen adsorption/desorption isotherms were collected and described by the Brunauer–Emmett–Teller (BET) and Barrett–Joyner–Halenda (BJH) models to derive specific surface area, pore volume, and pore size distribution values (Table 2). It can be observed that N/TiO<sub>2</sub> materials synthesized at different reaction times in the MW have a similar specific surface area, pore-volume, and average pore diameter, indicating that the reaction time on the MW oven does not have a significant effect on the porosity of the material. However, increasing the reaction temperature for a reaction time of 10 min (N/TiO<sub>2</sub> 150\_10 and N/TiO<sub>2</sub> 200\_10) results in an increase in specific surface area, pore volume, and average pore diameter. The FTIR spectra of the N/TiO<sub>2</sub> materials synthesized at different temperatures and reaction times are presented in Figure 1a. All materials show a strong wide band between 400 and 800 cm<sup>-1</sup>, which corresponds to the stretching vibrations of Ti–O–Ti bonds [39], whereas the broad band between 3650 and 2850 cm<sup>-1</sup>, and the peak at 1632 cm<sup>-1</sup>, are attributed to stretching vibrations of O–H group [40]. However, N/TiO<sub>2</sub> 150\_10 has additional peaks at 1590, 1525, 1443, and 1372 cm<sup>-1</sup>, which are ascribed to the stretching vibrations of C=O, N–H, and C–N groups, respectively, associated with the residual urea in the material [41]. While indicative for composition, FTIR hardly facilitates the selection of optimal reaction temperature and time. Figure 1b shows the X-ray diffraction patterns of N/TiO<sub>2</sub> materials synthesized at different temperatures and reaction times. All materials show diffraction peaks of TiO<sub>2</sub> anatase, assigned to the ICDD PDF#21–1272 [42]. It can be noticed that a higher treatment temperature is leading to narrower peaks, indicating larger crystallite size. Similar results were reported by Kadam et al. [43]. However, in this study, the anatase crystal phase is formed even at temperatures as low as 150 °C. Contrary to reaction temperature, the reaction time has a negligible effect on the crystal phase and the crystallite size (Figure 1b).

**Table 2.** Specific surface area, pore-volume, and crystallite size of N/TiO<sub>2</sub> materials.

Material	$S_{\text{BET}}, \text{m}^2 \text{g}^{-1}$	$V_{\text{pore}}, \text{cm}^3 \text{g}^{-1}$	Average Pore Diameter, nm
N/TiO <sub>2</sub> 150_10	172.4	0.260	5.46
N/TiO <sub>2</sub> 200_10	185.3	0.326	6.68
N/TiO <sub>2</sub> 200_20	187.8	0.342	6.91
N/TiO <sub>2</sub> 200_30	179.2	0.330	7.02

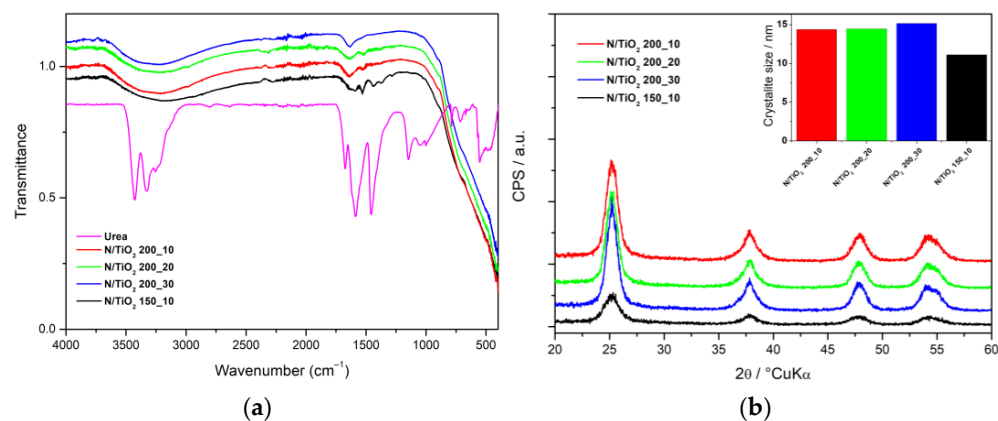


**Figure 1.** (a) FTIR spectra of N/TiO<sub>2</sub> materials, and (b) X-ray diffraction patterns, crystallite size.

### 3.2. Photocatalysis of N/TiO<sub>2</sub> for Optimization of the Reaction Time and Temperature

A photocatalytic experiment using the N/TiO<sub>2</sub> samples with constant N ratio was utilized for optimization of the sample preparation in terms of the reaction temperature and time, similarly to the characterization. The photocatalytic activity of the N/TiO<sub>2</sub> materials synthesized at different temperatures and reaction times was evaluated for the degradation of CIP aqueous solution (10 mg/L) under the UVA light and visible light, as shown in Figure 2. The photocatalytic experiments under the UV light (Figure 2a) show that N/TiO<sub>2</sub> materials synthesized at 200 °C degrade 90% of CIP in just 20 min of irradiation, while the material synthesized at 150 °C achieves less than 80% of removal at the same period. Additionally, it is noticed that materials synthesized at different reaction times (10, 20, and 30 min of MW oven treatment) have similar photoactivity, comparable to commercial Degussa P25 TiO<sub>2</sub>, achieving more than 95% degradation of CIP in only 45 min under the UV radiation with lamp (I). After 45 min, no noticeable CIP degradation changes are detected for materials synthesized at 200 °C, while the material synthesized at 150 °C requires more than 90 min to reach similar removal efficiency (Figure 2c). Under the visible light, all N/TiO<sub>2</sub> materials show some photoactivity under lamp III, while the photocatalyst Degussa P25 TiO<sub>2</sub> shows no activity at all (Figure 2b). The reason for photoactivity under the visible light is most likely the presence of nitrogen, which might cause the narrowing of the bandgap of TiO<sub>2</sub>, shifting its photo-responses to the visible spectrum [23,39]. In the CIP removal under both radiation sources, all synthesized materials show a synergistic effect of adsorption and photocatalysis, as shown in Figure 2c. The N/TiO<sub>2</sub> synthesized at 150 °C displays the highest adsorption capacity, which could be due to the affinity between amino or carboxylic group in the ciprofloxacin structure and the urea remaining in the material synthesized at 150 °C, as confirmed by the FTIR analysis. Despite the fact that the material synthesized at 150 °C displays a higher adsorption capacity, it has lower photoactivity than the materials synthesized at 200 °C. The materials synthesized at 200 °C and at different reaction times show similar photoactivity under both radiation sources (UVA and warm visible lights).

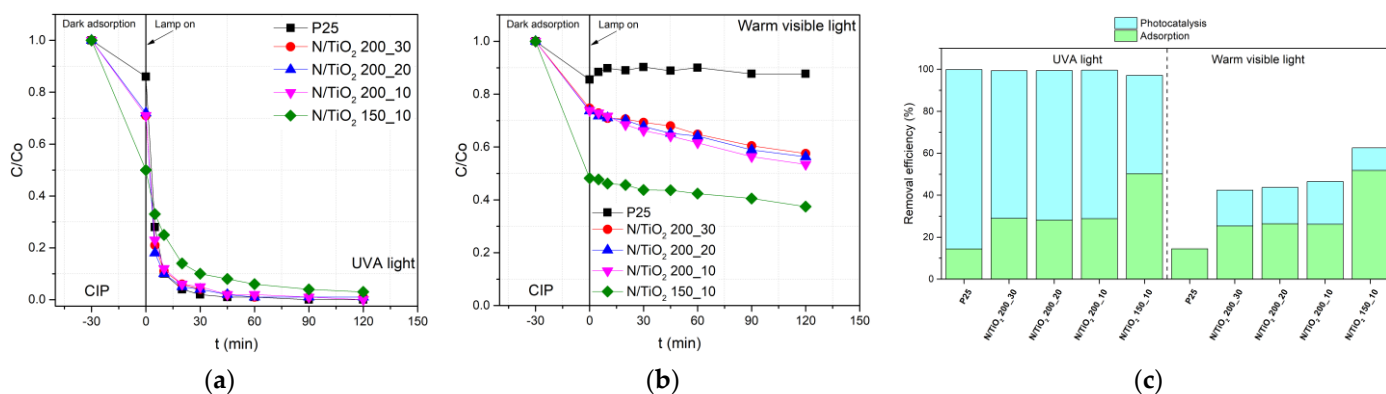


**Figure 2.** Photocatalytic degradation of ciprofloxacin (CIP) by Degussa P25 TiO<sub>2</sub> and N/TiO<sub>2</sub> materials under the (a) ultraviolet A (UVA) light (lamp I) and (b) warm visible light (lamp III). (c) CIP Removal efficiencies by Degussa P25 TiO<sub>2</sub> and N/TiO<sub>2</sub> materials under the UVA and warm visible lights.

Based on the characterization and photocatalytic results, the photoactivity is mainly affected by the size of the crystallite domains, which is governed by the synthesis temperature. The synthesis time marginally affected the morphological and photocatalytic properties. Therefore, 200 °C for 10 min is elucidated as the optimal MW oven treatment for further N/TiO<sub>2</sub> materials synthesis, where the amount of urea was optimized.

### 3.3. Bulk Characterization of N/TiO<sub>2</sub> for Optimization of the N Doping Amount

Following the elucidated optimal reaction time and temperature, we subjected the samples to broad structural, microstructural, and spectroscopic characterization in order

to optimize the preparing procedure in terms of the N content in the N/TiO<sub>2</sub> samples. The specific surface area, pore-volume, and average pore diameter of Degussa P-25 and N/TiO<sub>2</sub> materials synthesized at different N/Ti molar ratios are presented in Table 3. It can be noticed that the specific surface areas of N/TiO<sub>2</sub> materials are reduced while increasing the N/Ti ratio. The sample without urea (N/TiO<sub>2</sub> 0) presents the highest specific surface area. A similar reduction of the specific surface area with the increment of nitrogen ratio was reported by Ma et al. [44]. This reduction could be attributed to interstitial doping, in which nitrogen atoms could be located in the interstitial voids instead of crystal lattice sites [21]. Moreover, the specific surface areas of N/TiO<sub>2</sub> materials are significantly higher than the photocatalyst Degussa P-25 (up to four times higher). Interestingly, it can be observed that the pore volume and the average pore diameter are not significantly affected by the N/Ti ratio. For the case of N content variations, obviously, it is not as straightforward to determine the optimal content.

**Table 3.** Specific surface area, pore-volume, and pore size of N/TiO<sub>2</sub> materials and Degussa P25.

	$S_{\text{BET}}, \text{m}^2 \text{g}^{-1}$	$V_{\text{pore}}, \text{cm}^3 \text{g}^{-1}$	Average Pore Diameter, nm
N/TiO <sub>2</sub> 0	215.04	0.424	7.25
N/TiO <sub>2</sub> 1	144.40	0.273	7.26
N/TiO <sub>2</sub> 2	185.29	0.326	6.68
N/TiO <sub>2</sub> 4	158.09	0.295	7.19
N/TiO <sub>2</sub> 12	139.17	0.297	8.00
Degussa P25	48.14	0.196	13.69

In Figure 3a, the FTIR spectra of the N/TiO<sub>2</sub> materials and Degussa P25 are presented. A strong and wide band between 400 and 800 cm<sup>-1</sup> is observed for all materials, which can be associated with the stretching vibrations of Ti–O–Ti bonds. Additionally, the wide band between 3650 and 2850 cm<sup>-1</sup> and the peak at 1632 cm<sup>-1</sup> are correlated to stretching vibrations of the O–H group. Furthermore, in the N/TiO<sub>2</sub> materials containing a high N/Ti molar ratio (12 and 24), a small band around 1457 cm<sup>-1</sup> appears, which is attributed to the vibrations of the formed Ti–N bond [45]. Interestingly, all synthesized materials have a higher intensity of bands related to the O–H group than the P25 sample, which could be beneficial for the production of hydroxyl radicals during photocatalytic reactions [46,47]. The optimal N content can be hardly elucidated from the FTIR scans. The Raman spectra of the N/TiO<sub>2</sub> materials and commercial photocatalyst Degussa P25 are shown in Figure 3b. In general, for all materials, five peaks can be identified which are associated with the A<sub>1g</sub> (515 cm<sup>-1</sup>), B<sub>1g</sub> (396 cm<sup>-1</sup>) and E<sub>g</sub> (143, 396, and 637 cm<sup>-1</sup>) Raman modes of TiO<sub>2</sub> anatase phase [22,48], while, for the Degussa P25, an additional small peak at 444 cm<sup>-1</sup>, which is characteristic for the TiO<sub>2</sub> rutile phase, is observed [49]. In all N/TiO<sub>2</sub> synthesized materials (with and without urea), a slight shifting of the Raman peaks of the B<sub>1g</sub> and E<sub>g</sub> to higher wavenumbers is detected, and it could be attributed either to changes of surface oxygen vacancies or incorporation of nitrogen into the TiO<sub>2</sub> structure [24]. The Raman spectra indicate that nitrogen does not affect the crystallization of the TiO<sub>2</sub>. Figure 3c shows the X-ray diffraction patterns of N/TiO<sub>2</sub> materials and commercial photocatalyst Degussa P25. All synthesized N/TiO<sub>2</sub> materials display only diffraction peaks assigned to anatase (ICDD PDF#21–1272) [42], with crystallite size between 13 and 15 nm (determined by the Scherrer method); while the TiO<sub>2</sub> Degussa P25 exhibits diffraction peaks assigned to anatase (ICDD PDF#21–1272) and rutile (ICDD PDF#21–1276) [50], with average crystallite size of about 30 nm. In the materials containing urea, the anatase diffraction peak (101) is slightly shifted to lower angle ( $2\theta = 25.18^\circ$ ) compared to material without urea ( $2\theta = 25.41^\circ$ ), as shown in Figure 3d, and it could be associated with nitrogen doping [30]. Even though N content variations were used, there are no observable changes in the phase composition nor the crystallite size of the N/TiO<sub>2</sub> materials. Apart from the slight shifting of the diffraction

peak (101), no change is detected between materials with and without urea, proving the negligible structural effect of the nitrogen doping.

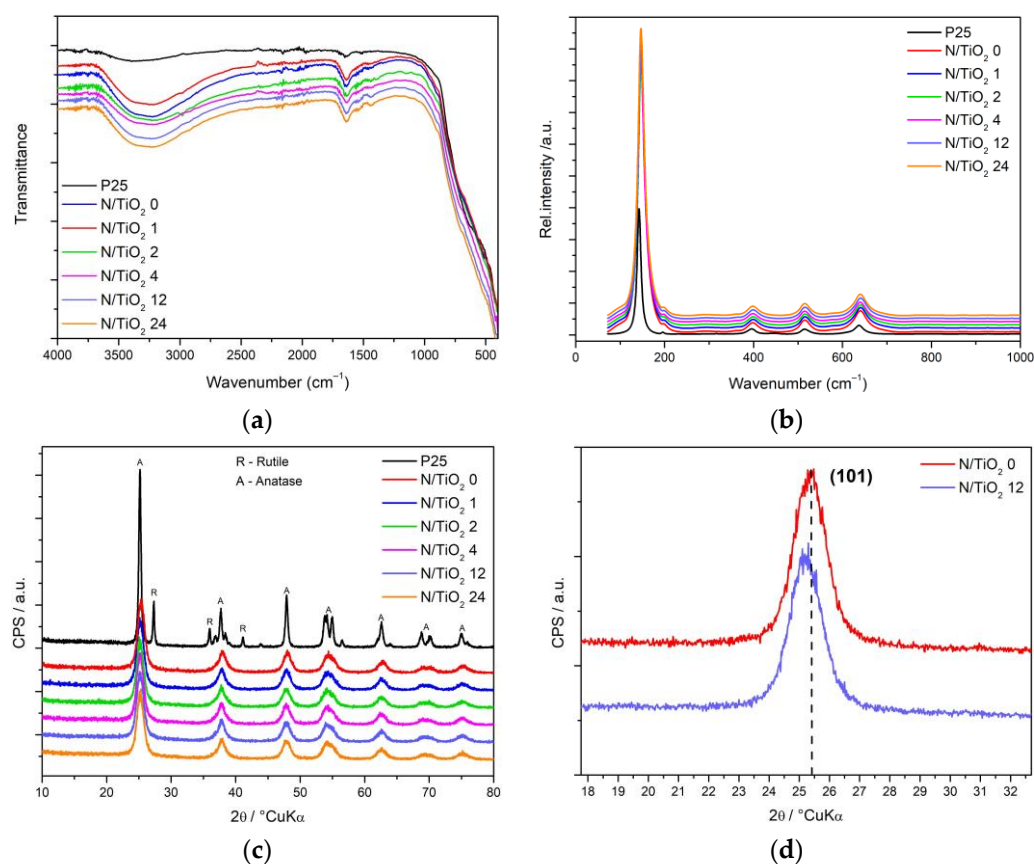


**Figure 3.** (a) FTIR spectra of N/TiO<sub>2</sub> materials and Degussa P25; (b) Raman spectra; (c) X-ray diffraction patterns, and; (d) X-ray diffraction peak (101) of the N/TiO<sub>2</sub> materials synthesized at 0 and 12 N/Ti molar ratios.

The SEM analysis was performed on the materials synthesized at 0 and 12 N/Ti molar ratios (Figure 4). Agglomerated particles having spherical shape are observed for both materials. It is observed that nitrogen addition does not have an effect on the morphology, shape, or size of the TiO<sub>2</sub> particles. In Figure 5, the fit of EDS analysis for materials synthesized at 0 and 12 N/Ti molar ratios, respectively, are presented. The Ti and O signals, which are typical in TiO<sub>2</sub>, are detected in both materials. Nitrogen traces are present even in the N/TiO<sub>2</sub> 0, which can be due to the nitrogen from the atmosphere because materials were stored at atmospheric conditions. In addition, it is well known that for values below 5%, quantitative analysis of the EDS spectra is less reliable. However, relatively more nitrogen is evident in the material N/TiO<sub>2</sub> 12. High-resolution EDS spectra were acquired precisely and fitted to allow more reliable quantitative results compared to conventional automated EDS analysis. Moreover, it is observed that EDS mapping of N for the material N/TiO<sub>2</sub> 12 points out a stronger and more homogeneous presence of N throughout the material, which is in line with the applied synthesis conditions.

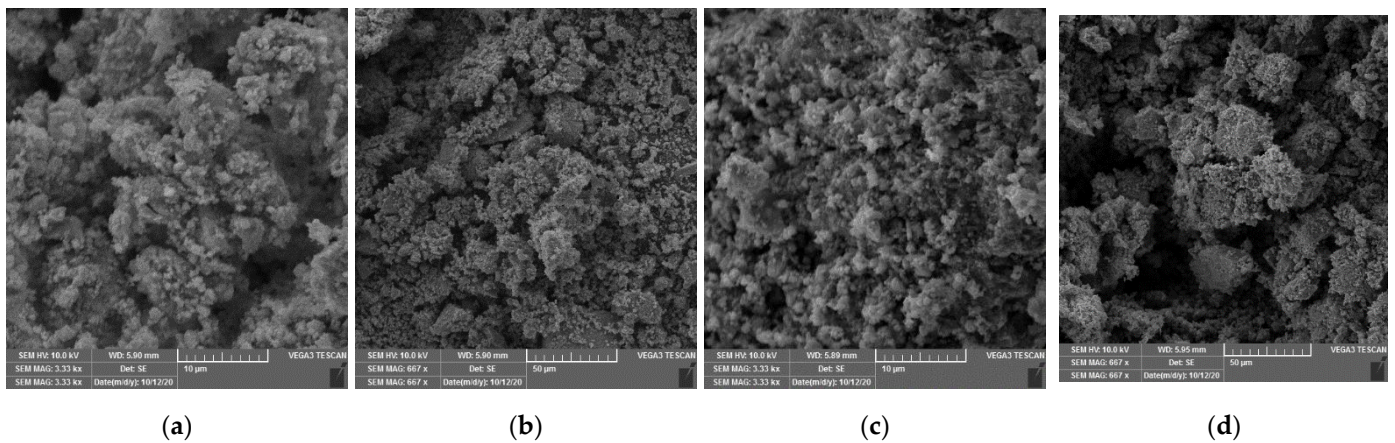


**Figure 4.** (a,b) SEM images of N/TiO<sub>2</sub> 0. (c,d) SEM images of N/TiO<sub>2</sub> 12.

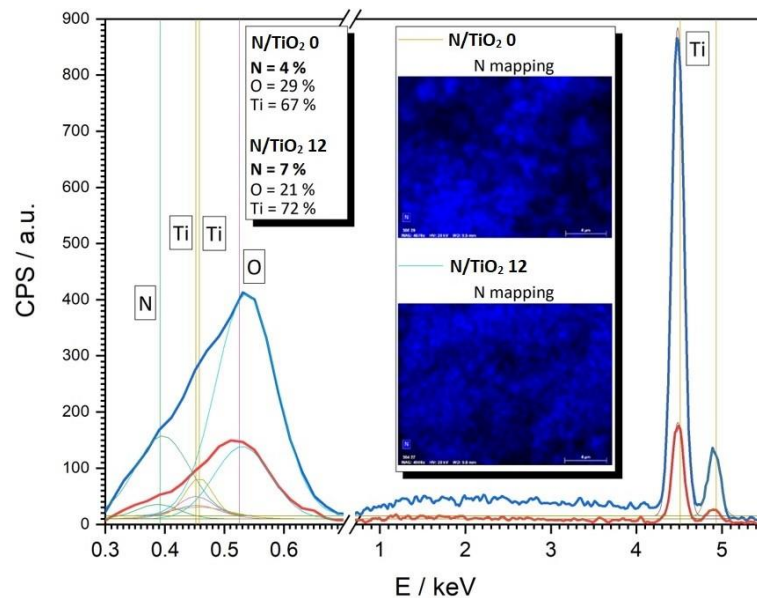


**Figure 5.** The fit of the EDS spectra for the N/TiO<sub>2</sub> 0 (4 atomic % of N) and N/TiO<sub>2</sub> 12 (7 atomic % of N). Inset: EDS mapping for the TiO<sub>2</sub> materials synthesized at 0 and 12 N/Ti molar ratios.

### 3.4. Surface Specific Characterization of N/TiO<sub>2</sub> for Optimization of the N Doping

In Figure 6, the high-resolution spectra of Ti, O, and N obtained by XPS measurements for N/TiO<sub>2</sub> 0 and N/TiO<sub>2</sub> 12 are shown, in which the chemical composition and oxidation states were determined. In Figure 6a,c, the O 1s spectra of materials N/TiO<sub>2</sub> 0 and N/TiO<sub>2</sub> 12, respectively, are shown. Three components with different binding energy values are observed in both materials, where the main peak at 530.1 eV is assigned to oxygen bonded to titanium (O-Ti). The peak at 532.8 eV is attributed to adsorbed oxygen, probably for O-H bonds of chemisorbed water [44]. Additionally, it is noticed that the peak related to chemisorbed water is slightly more intense in the sample N/TiO<sub>2</sub> 12, which favors the photocatalytic reactions due to the higher probability of generating of hydroxyl radicals. On the other hand, the third peak at 531.6 eV could be related to oxygen bonded to carbon, which could present impurities from the synthesis (urea or acetylacetone). Figure 6b,d show the Ti 2p spectra of materials N/TiO<sub>2</sub> 0 and N/TiO<sub>2</sub> 12. In both materials, two peaks at 458.8 eV and 464.5 eV, corresponding to Ti 2p<sup>1/2</sup> and Ti 2p<sup>3/2</sup>, are found. These two signals are evidence of the formation of the Ti<sup>4+</sup>, related to the anatase phase of TiO<sub>2</sub> [43,51,52]. Figure 6e represents N 1s spectrum recorded for N/TiO<sub>2</sub> 12. The small peak with binding energy of 400.15 eV is attributed to nitrogen bonded to oxygen (N-O) [45,53]. In general, it is assumed that the N 1s peak above 400 eV is related to interstitial

doping [24]. The introduction of nitrogen in the  $\text{TiO}_2$  lattice produces slight changes in the electronic densities of Ti and O. For the O 1s spectra, the main peak is shifted to lower binding energy from 530.1 to 529.95 eV; while for the Ti 2p spectra, the energy for the Ti  $2p^{1/2}$  is shifted to lower binding energy from 458.8 to 458.7 eV. The binding energy shifting is higher for the O 1s spectra due to N-O bonding. Usually, N-O bonding in the interstitial sites is achieved under wet chemical processes, which is the applied method used in the present study [54]. Although there are several techniques that can help to determine the presence of a doping element such as nitrogen, the XPS analysis is the most suitable technique for confirming the success of the doping process as well as the type of doping (substitutional or interstitial) [21].

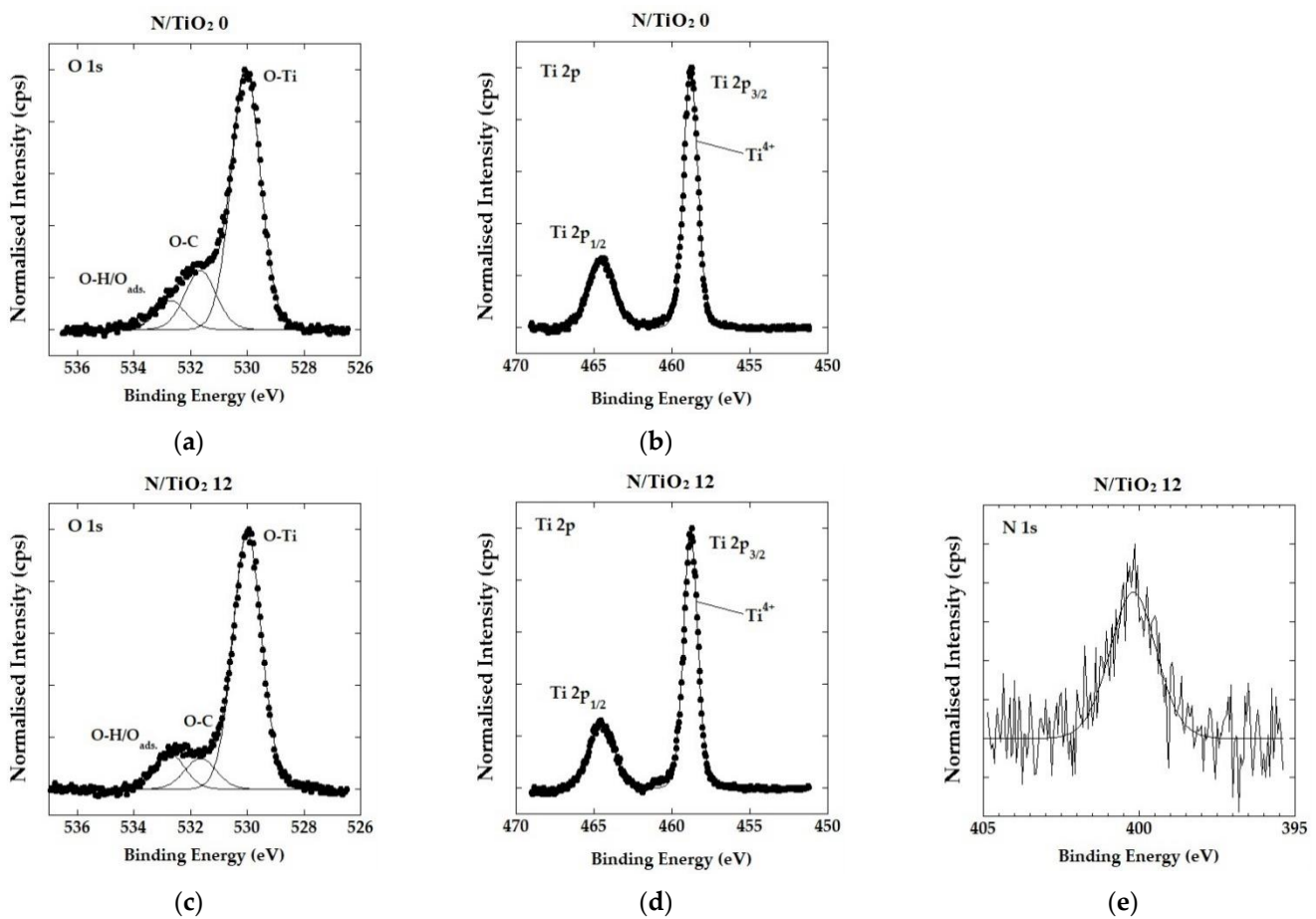


**Figure 6.** High-resolution XPS spectra: (a) O 1s spectrum, and; (b) Ti 2p spectrum, N/TiO<sub>2</sub> 0; (c) O 1s spectrum; (d) Ti 2p spectrum, and; (e) N 1s spectrum N/TiO<sub>2</sub> 12.

The DRS results and the Tauc plots are shown in Figure 7. From the DRS analysis (Figure 7a), it is observed that there are no significant differences in the energy absorption for the N/TiO<sub>2</sub> materials and Degussa P25. All materials only absorb photons at wavelengths shorter than 400 nm. Based on the DRS, the Tauc plots can be obtained to determine the energy bandgap of all materials (Figure 7b). It is noticed that all N/TiO<sub>2</sub> materials display a slight shift to the lower energy absorption in comparison to the Degussa P25. Additionally, it is observed that the increment in the N/Ti molar ratio increases the energy bandgap. Similar results were reported by Suwannaruang et al. [55]. The lowest energy bandgap is obtained for the material N/TiO<sub>2</sub> 0. The increment in the energy bandgap could be explained by the fact that the nitrogen is bonded to oxygen and it is introduced interstitially, as confirmed by XPS analysis, where nitrogen acts as an impurity, creating a new energetic level that contributes to the absorption in the visible light range without modifying the valence band (VB) or conduction band (CB) of TiO<sub>2</sub> [54,56]. Kuo et al. confirmed by density

functional theory calculations that band gap narrowing is achieved by substitutional nitrogen doping, while interstitial nitrogen doping produces localized impurities that do not reduce the energy band gap. However, both types of doping contributes to the absorption of photons in the visible range [56]. Previous studies have shown that a lower energy bandgap is not the only condition to achieve a higher photoactivity in the visible region. Other factors, such as oxygen vacancies and new energetic levels in the TiO<sub>2</sub> lattice, also play an important role in photocatalytic activity [50,54,55,57].

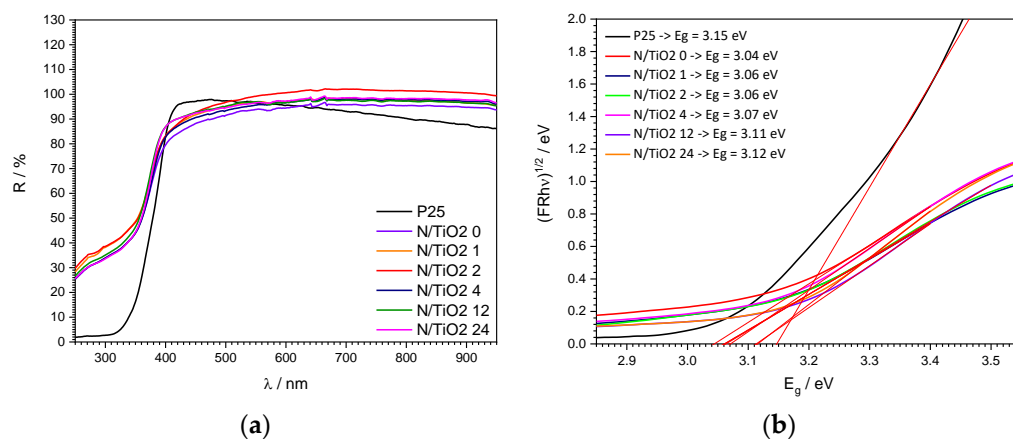


**Figure 7.** (a) DRS spectra and (b) Tauc plot for energy bandgap determination of N/TiO<sub>2</sub> materials and Degussa P25.

### 3.5. Photocatalytic Performance Experiment for N/TiO<sub>2</sub> Samples for Optimization of N Content

The photoactivity of the N/TiO<sub>2</sub> materials with the different N/Ti molar ratios, synthesized at 200 °C for 10 min in the MW oven, were evaluated again through the degradation of CIP aqueous solution (10 mg/L) under the UVA light (lamp I), solar light simulator (lamp II) and visible light (lamp III), as shown in Figure 8. In the Supplementary Materials, the additional photocatalytic degradation for materials with 1 and 2 N/Ti molar ratios (Figure S2) are shown. The photocatalytic data are described using the pseudo first-order and pseudo second-order models. The pseudo first-order model described a process where the degradation rate is affected mainly by the changes in pollutant concentration, while the pseudo second-order model described a process where the degradation rate is affected, besides the pollutant concentration, by other factors, such as light intensity or intermediates formation [58]. The kinetic constant for the pseudo first-order is obtained by the slope of the plot of  $-\ln(C/C_0)$  versus the irradiation time. For the pseudo second-order, the kinetic constant is obtained by the slope of the plot of  $(1/C - 1/C_0)$  versus the irradiation time. Analysis of the goodness of fit parameters for each model should point to one offering the better description of the process and thus better pointing out to reaction mechanism. Tables 4 and 5 show the pseudo first-order ( $k_1, \text{min}^{-1}$ ) and pseudo second-order kinetic constants ( $k_2, \text{L mg}^{-1} \text{min}^{-1}$ ) and removal efficiencies of N/TiO<sub>2</sub> materials. The pseudo first-order model shows that under the UV and solar light, the correlation coefficient ( $R^2$ ) in most of the cases has value below 0.90, indicating that the model does not describe well the experimental degradation process. On the contrary, the pseudo second order in all cases presents a correlation coefficient ( $R^2$ ) around 0.99, indicating that the model describes more precisely the degradation process under the UV and solar light. In the case of photocatalytic degradation under the visible light, although both models have a correlation coefficient ( $R^2$ ) above 0.90, the pseudo second-order fits better to the experimental results. From the photocatalytic tests, it is noticed that materials with a higher N/Ti molar ratio (12 and 24) and the photocatalyst Degussa P-25 achieve up to 90% CIP removal in just 20 min of UVA (lamp I) irradiation, while the materials with lower N/Ti molar ratio and N/TiO<sub>2</sub> 0 achieve less than 90% of removal in the same period. After 60 min of UVA irradiation, no significant changes in the CIP concentration are detected for all N/TiO<sub>2</sub> materials and

Degussa P-25 (Figure 8a). Moreover, it is noticed that by increasing N/Ti molar ratio, the degradation rate is increased, as displayed in Table 5. Under the SLS radiation (lamp II), similar behavior as under the UVA radiation is observed, where just 20 min of irradiation is required for all materials to achieve 90% of CIP removal. It is observed that an increment N/Ti molar ratio increases the degradation rate under the SLS radiation. However, the kinetic constants for all N/TiO<sub>2</sub> materials are higher under the SLS than under the UVA radiation. On the contrary, the commercial photocatalyst Degussa P-25 shows a lower kinetic constant under the SLS than under the UVA radiation (Table 5). The improvement in the kinetic constants under the SLS could be attributed to new energetic levels in the TiO<sub>2</sub> lattice due to the nitrogen doping, as confirmed by XPS analysis. The energetic levels due to nitrogen could shift the light absorption to the visible range and promote the charge separation, enhancing the photocatalytic activity under the solar spectrum [21,48]. On the other hand, the maximum degradation rate is achieved for the N/TiO<sub>2</sub> 12 under the UVA (lamp I) and solar radiation (lamp II). Having a N/Ti molar ratio higher than 12, the kinetic constant decreases due to the fact that nitrogen excess could act as a recombination center that reduces photocatalytic activity [44]. The CIP degradation under the warm visible light (lamp III) shows that all N/TiO<sub>2</sub> materials have photocatalytic activity, while the commercial TiO<sub>2</sub> does not show photoactivity under this irradiation source (Figure 8c). Again, it is observed that photoactivity rate increases when N/Ti molar ratio also increases. However, after 120 min of irradiation, any N/TiO<sub>2</sub> material achieves a complete CIP removal under this radiation source. This could be explained by the fact that the photons emitted by the lamp III are mainly from the wavelength around 600 nm, and just a small portion of photons are emitted at 450 nm (Figure S1), making the kinetic constants 100 times lower than under the SLS. Therefore, a longer irradiation period could be required to achieve complete CIP removal.

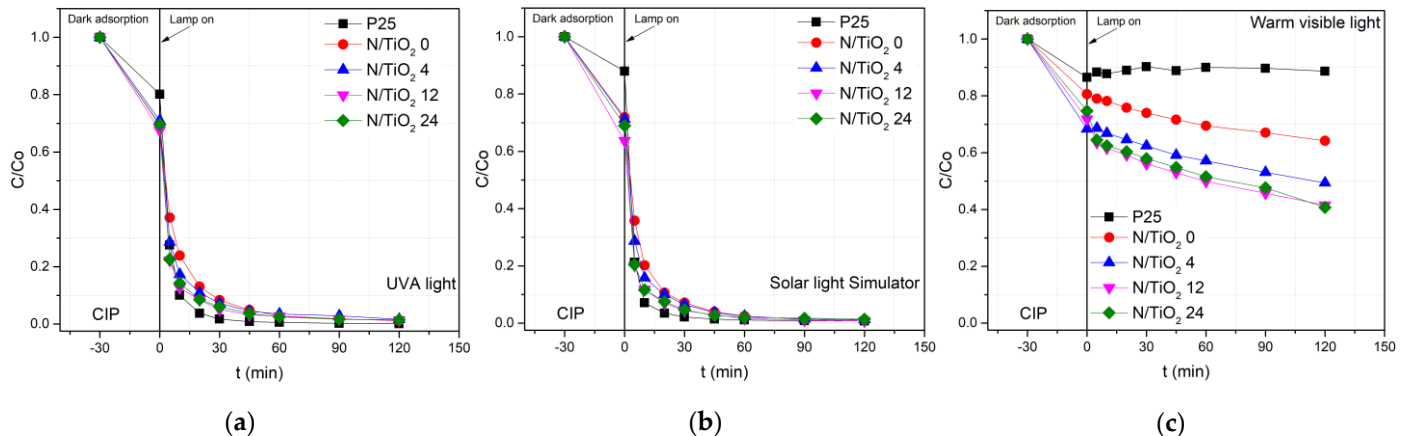


**Figure 8.** Photocatalytic degradation of ciprofloxacin by Degussa P25 TiO<sub>2</sub> and N/TiO<sub>2</sub> materials under (a) UVA light (lamp I), (b) Solar light simulator lamp (II), and (c) warm visible light (lamp III).

**Table 4.** Parameters obtained from the ciprofloxacin (CIP) degradation under UVA (lamp I), Solar light simulator (lamp II), and warm visible light (lamp III) fitted to a pseudo-first-order kinetic model for N/TiO<sub>2</sub> materials.

Lamp	$k_1, (\text{min}^{-1})$			$R^2$		
	I	II	III	I	II	III
N/TiO <sub>2</sub> 0	0.0380	0.0432	0.0021	0.9001	0.9023	0.9796
N/TiO <sub>2</sub> 4	0.0406	0.0443	0.0028	0.8893	0.8928	0.9957
N/TiO <sub>2</sub> 12	0.0432	0.0477	0.0053	0.8635	0.8843	0.9432
N/TiO <sub>2</sub> 24	0.0425	0.0464	0.0055	0.8621	0.8673	0.9392
Degussa P25	0.0588	0.0563	-	0.8562	0.8187	-

**Table 5.** Parameters obtained from the CIP degradation under UVA (lamp I), Solar light simulator (lamp II), and warm visible light (lamp III) fitted to a pseudo-second-order kinetic model, and removal efficiency of N/TiO<sub>2</sub> materials.

Lamp	$k_2$ , (L mg <sup>-1</sup> min <sup>-1</sup> )			$R^2$			Removal Efficiency ( $\eta$ )		
	I	II	III	I	II	III	I	II	III
N/TiO <sub>2</sub> 0	0.3905	0.5750	0.0028	0.9959	0.9909	0.9861	98.07%	98.68%	35.83%
N/TiO <sub>2</sub> 4	0.4798	0.6499	0.0044	0.9946	0.9886	0.9978	98.46%	98.78%	50.64%
N/TiO <sub>2</sub> 12	0.5881	0.9768	0.0088	0.9975	0.9869	0.9687	98.66%	99.21%	58.51%
N/TiO <sub>2</sub> 24	0.5376	0.7852	0.0091	0.9872	0.9974	0.9655	98.40%	99.02%	59.26%
Degussa P25	1.7868	1.2320	-	0.9907	0.9948	-	99.61%	99.35%	12.32% *

\* By adsorption process.

### 3.6. Determining the Relation Adsorption/Photocatalytic Removal of CIP for Different Irradiation Sources

Under the three different radiation sources, a synergistic effect of adsorption and the photocatalytic process takes place for CIP removal, as shown in Figures 8 and 9. Regardless of the N/Ti molar ratio, all N/TiO<sub>2</sub> materials display similar adsorption capacity, where the adsorption process represents around 30% of CIP removal. This similar adsorption capacity is related to the high specific surface area of all N/TiO<sub>2</sub> materials and due to the affinity of the amine and carboxylic groups of CIP with the hydroxyl groups in the surface of the materials, favoring the adsorption of the pollutant on the photocatalyst surface. Comparing and evaluating the results from different models (pseudo first-order and pseudo second-order) leads to the conclusion that the photocatalytic degradation of CIP by the N/TiO<sub>2</sub> materials follows the second order kinetic model, similar to the results reported by Gabelica et al. [28]. The pseudo first-order and pseudo second-order kinetic plots of CIP photocatalytic degradation by Degussa P25 TiO<sub>2</sub> and N/TiO<sub>2</sub> materials are given in Figures S3 and S4, respectively.

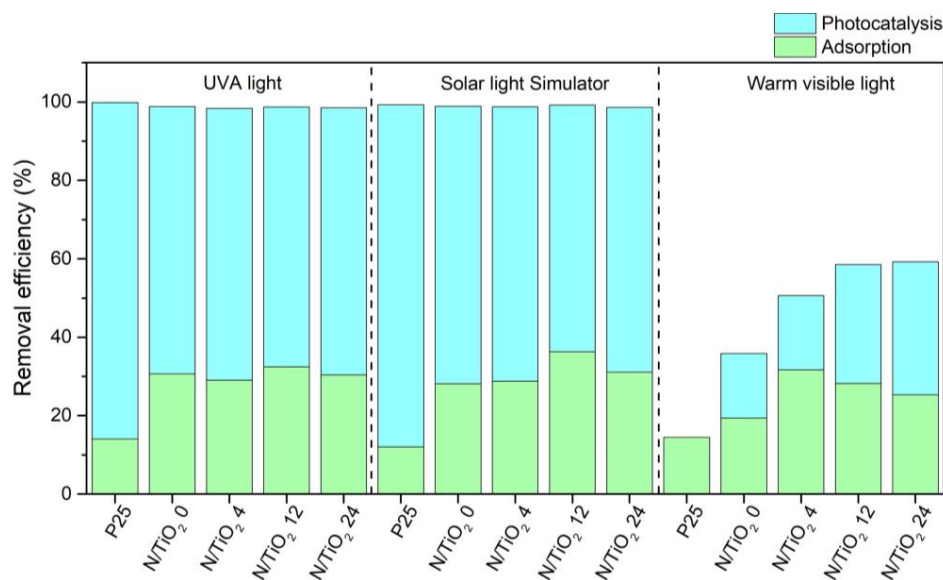


**Figure 9.** CIP removal efficiencies by Degussa P25 TiO<sub>2</sub> and N/TiO<sub>2</sub> materials under UVA light (lamp I), Solar light simulator lamp (II), and warm visible light (lamp III).

## 4. Conclusions

Here, we demonstrate the successful utilization of the microwave-assisted synthesis for the purpose of preparing nitrogen doped titania nanoparticles. This non-conventional approach has proven advantages on the basis of a documented reduction of the environmental impact due to the reduction of necessary energy, solvent, and stabilizers compared to majority of other wet-chemistry synthesis techniques. We employed a strategy for

preparing, characterizing, and optimizing the preparation in two cycles, for the purpose of selecting the best reaction temperature, time, and N content. Samples are crystallized as anatase without subsequent thermal treatment, and the reaction temperature was identified as the main quality parameter. On the other hand, the change of the composition, i.e., precursor ratio, hardly influenced the morphology of the samples. However, N content was important for photocatalytic performance.

The photocatalytic activity of N/TiO<sub>2</sub> nanoparticle containing aqueous suspensions was evaluated for the degradation of antibiotic ciprofloxacin (CIP) under different irradiation spectra: UVA, simulated solar light, and visible light. For all experiment conditions and samples investigated, the degradation performance was efficient and relatively aligned. Increasing the synthesis temperature and nitrogen content seems to be beneficial for increasing the degradation efficiency up to a point of saturation, after which nitrogen can act as a recombination center. Finally, the overall best material proved to be TiO<sub>2</sub> derived at 200 °C for 10 min, having an intermediate N/Ti molar ratio of up to 12 using the synergy of three irradiation sources.

**Supplementary Materials:** The following are available online at <https://www.mdpi.com/article/10.3390/nano12091473/s1>, Figure S1: Radiation spectra of three different lamps: (a) warm visible light, (b) Solar light, and (c) UVA. (d) UV/Vis Absorbance spectrum of ciprofloxacin (CIP), Figure S2: Photocatalytic degradation of ciprofloxacin by Degussa P25 TiO<sub>2</sub> and N/TiO<sub>2</sub> samples under (a) UVA light (lamp I), (b) Solar light simulator lamp (II), and (c) warm visible light (lamp III), Figure S3: Pseudo-first-order kinetic rate of the photocatalytic degradation of ciprofloxacin by Degussa P25 TiO<sub>2</sub> and N/TiO<sub>2</sub> samples under (a) UVA light (lamp I), (b) Solar light simulator lamp (II), and (c) warm visible light (lamp III), Figure S4: Pseudo-second-order kinetic rate of the photocatalytic degradation of ciprofloxacin by Degussa P25 TiO<sub>2</sub> and N/TiO<sub>2</sub> samples under (a) UVA light (lamp I), (b) Solar light simulator lamp (II), and (c) warm visible light (lamp III).

**Author Contributions:** Conceptualization, C.S.T., D.L., L.Ć. and V.M.; methodology, C.S.T., D.L., L.Ć. and V.M.; software, C.S.T., D.L. and V.M.; validation, C.S.T., D.L., L.Ć., I.P., G.M. and V.M.; formal analysis, C.S.T., V.M., I.P. and G.M.; investigation, C.S.T.; resources, L.Ć., D.L. and V.M.; data curation, C.S.T., D.L., L.Ć., I.P., G.M. and V.M.; writing—original draft preparation, C.S.T., D.L., L.Ć., I.P. and V.M.; writing—review and editing, C.S.T., D.L., L.Ć., I.P., G.M. and V.M.; visualization, C.S.T., D.L., L.Ć. and V.M.; supervision, D.L. and L.Ć.; project administration, L.Ć. and D.L.; funding acquisition, L.Ć. and D.L. All authors have read and agreed to the published version of the manuscript.

**Funding:** This research was funded by the European Union’s Horizon 2020 research and innovation programme under the Marie Skłodowska Curie grant agreement 812880; NOWELTIES project.

**Data Availability Statement:** The data presented in this study are available upon reasonable request from the corresponding author.

**Conflicts of Interest:** The authors declare no conflict of interest.

## References

1. Patel, M.; Kumar, R.; Kishor, K.; mLsna, T.; Pittman, C.U.; Mohan, D. Pharmaceuticals of Emerging Concern in Aquatic Systems: Chemistry, Occurrence, Effects, and Removal Methods. *Chem. Rev.* **2019**, *119*, 3510–3673. [[CrossRef](#)] [[PubMed](#)]
2. Wilkinson, J.; Hooda, P.S.; Barker, J.; Barton, S.; Swinden, J. Occurrence, fate and transformation of emerging contaminants in water: An overarching review of the field. *Environ. Pollut.* **2017**, *231*, 954–970. [[CrossRef](#)] [[PubMed](#)]
3. Morin-Crini, N.; Lichtfouse, E.; Fourmentin, M.; Ribeiro, A.R.L.; Noutsopoulos, C.; Mapelli, F.; Fenyvesi, É.; Vieira, M.G.A.; Picos-Corrales, L.A.; Moreno-Piraján, J.C.; et al. *Remediation of Emerging Contaminants*; Morin-Crini, N., Lichtfouse, E., Crini, G., Eds.; Springer: Cham, Switzerland, 2021; pp. 1–106. [[CrossRef](#)]
4. Cui, N.; Zada, A.; Song, J.; Yang, Y.; Liu, M.; Wang, Y.; Wu, Y.; Qi, K.; Selvaraj, R.; Liu, S.Y.; et al. Plasmon-induced ZnO-Ag/AgCl photocatalyst for degradation of tetracycline hydrochloride. *Desalin. Water Treat.* **2022**, *245*, 247–254. [[CrossRef](#)]
5. Zhang, Z.; Zada, A.; Cui, N.; Liu, N.; Liu, M.; Yang, Y.; Jiang, D.; Jiang, J.; Liu, S. Synthesis of ag loaded ZnO/BiOCl with high photocatalytic performance for the removal of antibiotic pollutants. *Crystals* **2021**, *11*, 981. [[CrossRef](#)]
6. Krzeminski, P.; Tomei, M.C.; Karaolia, P.; Langenhoff, A.; Almeida, C.M.R.; Felis, E.; Gritten, F.; Andersen, H.R.; Fernandes, T.; Manaia, C.M.; et al. Performance of secondary wastewater treatment methods for the removal of contaminants of emerging concern implicated in crop uptake and antibiotic resistance spread: A review. *Sci. Total Environ.* **2019**, *648*, 1052–1081. [[CrossRef](#)]

7. Kutuzova, A.; Dontsova, T.; Kwapinski, W. Application of TiO<sub>2</sub>-Based Photocatalysts to Antibiotics Degradation: Cases of Sulfamethoxazole, Trimethoprim and Ciprofloxacin. *Catalysts* **2021**, *11*, 728. [[CrossRef](#)]
8. Radović Vučić, M.; Baošić, R.; Mitrović, J.; Petrović, M.; Velinov, N.; Kostić, M.; Bojić, A. Comparison of the advanced oxidation processes in the degradation of pharmaceuticals and pesticides in simulated urban wastewater: Principal component analysis and energy requirements. *Process Saf. Environ. Prot.* **2021**, *149*, 786–793. [[CrossRef](#)]
9. Wang, J.; Zhuan, R. Degradation of antibiotics by advanced oxidation processes: An overview. *Sci. Total Environ.* **2020**, *701*, 135023. [[CrossRef](#)]
10. Wang, J.; Wang, S. Removal of pharmaceuticals and personal care products (PPCPs) from wastewater: A review. *J. Environ. Manag.* **2016**, *182*, 620–640. [[CrossRef](#)]
11. Kanakaraju, D.; Glass, B.D.; Oelgemöller, M. Advanced oxidation process-mediated removal of pharmaceuticals from water: A review. *J. Environ. Manag.* **2018**, *219*, 189–207. [[CrossRef](#)]
12. Ansari, S.A.; Khan, M.M.; Ansari, M.O.; Cho, M.H. Nitrogen-doped titanium dioxide (N-doped TiO<sub>2</sub>) for visible light photocatalysis. *New J. Chem.* **2016**, *40*, 3000–3009. [[CrossRef](#)]
13. Truppi, A.; Petronella, F.; Placido, T.; Striccoli, M.; Agostiano, A.; Curri, M.L.; Comparelli, R. Visible-light-active TiO<sub>2</sub>-based hybrid nanocatalysts for environmental applications. *Catalysts* **2017**, *7*, 100. [[CrossRef](#)]
14. Šegota, S.; Ćurković, L.; Ljubas, D.; Svetličić, V.; Houra, I.F.; Tomašić, N. Synthesis, characterization and photocatalytic properties of sol-gel TiO<sub>2</sub> films. *Ceram. Int.* **2011**, *37*, 1153–1160. [[CrossRef](#)]
15. Dong, H.; Zeng, G.; Tang, L.; Fan, C.; Zhang, C.; He, X.; He, Y. An overview on limitations of TiO<sub>2</sub>-based particles for photocatalytic degradation of organic pollutants and the corresponding countermeasures. *Water Res.* **2015**, *79*, 128–146. [[CrossRef](#)]
16. Etacheri, V.; Di Valentin, C.; Schneider, J.; Bahnemann, D.; Pillai, S.C. Visible-light activation of TiO<sub>2</sub> photocatalysts: Advances in theory and experiments. *J. Photochem. Photobiol. C Photochem. Rev.* **2015**, *25*, 1–29. [[CrossRef](#)]
17. Shayegan, Z.; Lee, C.S.; Haghghat, F. TiO<sub>2</sub> photocatalyst for removal of volatile organic compounds in gas phase—A review. *Chem. Eng. J.* **2018**, *334*, 2408–2439. [[CrossRef](#)]
18. Zada, A.; Khan, M.; Hussain, Z.; Shah, M.I.A.; Ateeq, M.; Ullah, M.; Ali, N.; Shaheen, S.; Yasmeen, H.; Ali Shah, S.N.; et al. Extended visible light driven photocatalytic hydrogen generation by electron induction from g-C<sub>3</sub>N<sub>4</sub> nanosheets to ZnO through the proper heterojunction. *Z. Phys. Chem.* **2022**, *236*, 53–66. [[CrossRef](#)]
19. Schneider, J.; Matsuoka, M.; Takeuchi, M.; Zhang, J.; Horiuchi, Y.; Anpo, M.; Bahnemann, D.W. Understanding TiO<sub>2</sub> photocatalysis: Mechanisms and materials. *Chem. Rev.* **2014**, *114*, 9919–9986. [[CrossRef](#)]
20. Piątkowska, A.; Janus, M.; Szymański, K.; Mozia, S. C-, N- and S-Doped TiO<sub>2</sub> Photocatalysts: A Review. *Catalysts* **2021**, *11*, 144. [[CrossRef](#)]
21. Ding, W.; Li, W. A first principles study of the energetics and core level shifts of anion-doped TiO<sub>2</sub> photocatalysts. *Chin. J. Catal.* **2014**, *36*, 181–187. [[CrossRef](#)]
22. Brindha, A.; Sivakumar, T. Visible active N, S co-doped TiO<sub>2</sub>/graphene photocatalysts for the degradation of hazardous dyes. *J. Photochem. Photobiol. A Chem.* **2017**, *340*, 146–156. [[CrossRef](#)]
23. Natarajan, T.S.; Mozhiarasi, V.; Tayade, R.J. Nitrogen Doped Titanium Dioxide (N-TiO<sub>2</sub>): Synopsis of Synthesis Methodologies, Doping Mechanisms, Property Evaluation and Visible Light Photocatalytic Applications. *Photochem* **2021**, *1*, 371–410. [[CrossRef](#)]
24. Gomes, J.; Lincho, J.; Domingues, E.; Quinta-Ferreira, R.; Martins, R. N-TiO<sub>2</sub> Photocatalysts: A Review of Their Characteristics and Capacity for Emerging Contaminants Removal. *Water* **2019**, *11*, 373. [[CrossRef](#)]
25. Suwannaruang, T.; Hildebrand, J.P.; Taffa, D.H.; Wark, M.; Kamonsuangkasem, K.; Chirawatkul, P.; Wantala, K. Visible light-induced degradation of antibiotic ciprofloxacin over Fe-N-TiO<sub>2</sub> mesoporous photocatalyst with anatase/rutile/brookite nanocrystal mixture. *J. Photochem. Photobiol. A Chem.* **2020**, *391*, 112371. [[CrossRef](#)]
26. Catauro, M.; Tranquillo, E.; Dal Poggetto, G.; Pasquali, M.; Dell’Era, A.; Cipriotti, S.V. Influence of the heat treatment on the particles size and on the crystalline phase of TiO<sub>2</sub> synthesized by the sol-gel method. *Materials* **2018**, *11*, 2364. [[CrossRef](#)]
27. Xi, J.; Zhang, Y.; Chen, X.; Hu, Y. A simple sol-gel hydrothermal method for the synthesis of defective TiO<sub>2</sub> nanocrystals with excellent visible-light photocatalytic activity. *Res. Chem. Intermed.* **2020**, *46*, 2205–2214. [[CrossRef](#)]
28. Gabelica, I.; Ćurković, L.; Mandić, V.; Panžić, I.; Ljubas, D.; Zadro, K. Rapid microwave-assisted synthesis of Fe<sub>3</sub>O<sub>4</sub>/SiO<sub>2</sub>/TiO<sub>2</sub> core-2-layer-shell nanocomposite for photocatalytic degradation of ciprofloxacin. *Catalysts* **2021**, *11*, 1136. [[CrossRef](#)]
29. Blanco-Vega, M.P.; Guzmán-Mar, J.L.; Villanueva-Rodríguez, M.; Maya-Treviño, L.; Garza-Tovar, L.L.; Hernández-Ramírez, A.; Hinojosa-Reyes, L. Photocatalytic elimination of bisphenol A under visible light using Ni-doped TiO<sub>2</sub> synthesized by microwave assisted sol-gel method. *Mater. Sci. Semicond. Process.* **2017**, *71*, 275–282. [[CrossRef](#)]
30. Mendiola-Alvarez, S.Y.; Guzmán-Mar, J.L.; Turnes-Palomino, G.; Maya-Alejandro, F.; Hernández-Ramírez, A.; Hinojosa-Reyes, L. UV and visible activation of Cr(III)-doped TiO<sub>2</sub> catalyst prepared by a microwave-assisted sol-gel method during MCPA degradation. *Environ. Sci. Pollut. Res.* **2017**, *24*, 12673–12682. [[CrossRef](#)]
31. Paluch, K.J.; McCabe, T.; Müller-Bunz, H.; Corrigan, O.I.; Healy, A.M.; Tajber, L. Formation and physicochemical properties of crystalline and amorphous salts with different stoichiometries formed between ciprofloxacin and succinic acid. *Mol. Pharm.* **2013**, *10*, 3640–3654. [[CrossRef](#)]
32. Sanchis-Perucho, A.; Orts-Arroyo, M.; Camús-Hernández, J.; Rojas-Dotti, C.; Escrivà, E.; Lloret, F.; Martínez-Lillo, J. Hexahalorhenate(IV) salts of protonated ciprofloxacin: Antibiotic-based single-ion magnets. *CrystEngComm* **2021**, *23*, 8579–8587. [[CrossRef](#)]

33. Golovnev, N.N.; Molokeyev, M.S.; Lesnikov, M.K.; Atuchin, V.V. Two salts and the salt cocrystal of ciprofloxacin with thiobarbituric and barbituric acids: The structure and properties. *J. Phys. Org. Chem.* **2018**, *31*, e3773. [[CrossRef](#)]
34. Commission Implementing Decision (EU) 2018/840 of 5 June 2018 Establishing a Watch List of Substances for Union-Wide Monitoring in the Field of Water Policy Pursuant to Directive 2008/105/EC of the European Parliament and of the Council and Repealing Commission Implementing Decision (EU) 2015/495 (Notified under Document C(2018) 3362). *Off. J. Eur. Union* **2018**, *L141*, 9–12.
35. Commission Implementing Decision (EU) 2020/1161 of 4 August 2020 Establishing a Watch List of Substances for Union-Wide Monitoring in the Field of Water Policy Pursuant to Directive 2008/105/EC of the European Parliament and of the Council (Notified under Document Number C(2020) 5205). *Off. J. Eur. Union* **2020**, *L257*, 32–35.
36. Malakootian, M.; Faraji, M.; Malakootian, M.; Nozari, M. Ciprofloxacin removal from aqueous media by adsorption process: A systematic review and meta-analysis. *Desalin. Water Treat.* **2021**, *229*, 252–282. [[CrossRef](#)]
37. Do, M.T.; Stuckey, D.C. Fate and removal of Ciprofloxacin in an anaerobic membrane bioreactor (AnMBR). *Bioresour. Technol.* **2019**, *289*, 121683. [[CrossRef](#)]
38. Thapa, R.; Maiti, S.; Rana, T.H.; Maiti, U.N.; Chattopadhyay, K.K. Anatase TiO<sub>2</sub> nanoparticles synthesis via simple hydrothermal route: Degradation of Orange II, Methyl Orange and Rhodamine B. *J. Mol. Catal. A Chem.* **2012**, *363–364*, 223–229. [[CrossRef](#)]
39. Cheng, X.; Yu, X.; Xing, Z.; Yang, L. Synthesis and characterization of N-doped TiO<sub>2</sub> and its enhanced visible-light photocatalytic activity. *Arab. J. Chem.* **2016**, *9*, S1706–S1711. [[CrossRef](#)]
40. Sher Shah, M.S.A.; Park, A.R.; Zhang, K.; Park, J.H.; Yoo, P.J. Green synthesis of biphasic TiO<sub>2</sub>-reduced graphene oxide nanocomposites with highly enhanced photocatalytic activity. *ACS Appl. Mater. Interfaces* **2012**, *4*, 3893–3901. [[CrossRef](#)]
41. Factorovich, M.; Guz, L.; Candal, R. N-TiO<sub>2</sub>: Chemical synthesis and photocatalysis. *Adv. Phys. Chem.* **2011**, *2011*. [[CrossRef](#)]
42. Švagelj, Z.; Mandić, V.; Čurković, L.; Biošić, M.; Žmak, I.; Gaborardi, M. Titania-Coated alumina foam photocatalyst for memantine degradation derived by replica method and sol-gel reaction. *Materials* **2020**, *13*, 227. [[CrossRef](#)] [[PubMed](#)]
43. Kadam, A.N.; Dhabbe, R.S.; Kokate, M.R.; Gaikwad, Y.B.; Garadkar, K.M. Preparation of N doped TiO<sub>2</sub> via microwave-assisted method and its photocatalytic activity for degradation of Malathion. *Spectrochim. Acta Part A Mol. Biomol. Spectrosc.* **2014**, *133*, 669–676. [[CrossRef](#)] [[PubMed](#)]
44. Ma, X.; Hao, K.; Dai, Y.; Song, L.; Yu, Q.; Yin, X.; Wang, Z. Enhanced Visible-Light Photocatalytic Activity by the Comprehensive Effects of Mesoporous and N-Doping at the Meso-N-TiO<sub>2</sub> Nanocatalysts. *ChemistrySelect* **2021**, *6*, 6029–6036. [[CrossRef](#)]
45. Yang, G.; Jiang, Z.; Shi, H.; Xiao, T.; Yan, Z. Preparation of highly visible-light active N-doped TiO<sub>2</sub> photocatalyst. *J. Mater. Chem.* **2010**, *20*, 5301–5309. [[CrossRef](#)]
46. Barkul, R.P.; Koli, V.B.; Shewale, V.B.; Patil, M.K.; Delekar, S.D. Visible active nanocrystalline N-doped anatase TiO<sub>2</sub> particles for photocatalytic mineralization studies. *Mater. Chem. Phys.* **2016**, *173*, 42–51. [[CrossRef](#)]
47. Chung, K.H.; Kim, B.J.; Park, Y.K.; Kim, S.C.; Jung, S.C. Photocatalytic properties of amorphous n-doped TiO<sub>2</sub> photocatalyst under visible light irradiation. *Catalysts* **2021**, *11*, 1010. [[CrossRef](#)]
48. Madurai Ramakrishnan, V.; Sandberg, S.; Muthukumarasamy, N.; Kvamme, K.; Balraju, P.; Agilan, S.; Velauthapillai, D. Microwave-assisted solvothermal synthesis of worms-like TiO<sub>2</sub> nanostructures in submicron regime as light scattering layers for dye-sensitized solar cells. *Mater. Lett.* **2019**, *236*, 747–751. [[CrossRef](#)]
49. Russo, P.; Liang, R.; He, R.X.; Zhou, Y.N. Phase transformation of TiO<sub>2</sub> nanoparticles by femtosecond laser ablation in aqueous solutions and deposition on conductive substrates. *Nanoscale* **2017**, *9*, 6167–6177. [[CrossRef](#)]
50. Bakre, P.V.; Tilve, S.G.; Shirsat, R.N. Influence of N sources on the photocatalytic activity of N-doped TiO<sub>2</sub>. *Arab. J. Chem.* **2020**, *13*, 7637–7651. [[CrossRef](#)]
51. Kocijan, M.; Čurković, L.; Radošević, T.; Podlogar, M. Enhanced photocatalytic activity of hybrid rGO@TiO<sub>2</sub>/CN nanocomposite for organic pollutant degradation under solar light irradiation. *Catalysts* **2021**, *11*, 1023. [[CrossRef](#)]
52. Atuchin, V.V.; Kesler, V.G.; Pervukhina, N.V.; Zhang, Z. Ti 2p and O 1s core levels and chemical bonding in titanium-bearing oxides. *J. Electron Spectrosc. Relat. Phenom.* **2006**, *152*, 18–24. [[CrossRef](#)]
53. Nolan, N.T.; Synnott, D.W.; Seery, M.K.; Hinder, S.J.; Van Wassenhoven, A.; Pillai, S.C. Effect of N-doping on the photocatalytic activity of sol-gel TiO<sub>2</sub>. *J. Hazard. Mater.* **2012**, *211–212*, 88–94. [[CrossRef](#)] [[PubMed](#)]
54. Asahi, R.; Morikawa, T.; Irie, H.; Ohwaki, T. Nitrogen-doped titanium dioxide as visible-light-sensitive photocatalyst: Designs, developments, and prospects. *Chem. Rev.* **2014**, *114*, 9824–9852. [[CrossRef](#)] [[PubMed](#)]
55. Suwannaruang, T.; Kidkhunthod, P.; Chanlek, N.; Soontaranon, S.; Wantala, K. High anatase purity of nitrogen-doped TiO<sub>2</sub> nanorice particles for the photocatalytic treatment activity of pharmaceutical wastewater. *Appl. Surf. Sci.* **2019**, *478*, 1–14. [[CrossRef](#)]
56. Kuo, C.L.; Chen, W.G.; Chen, T.Y. The electronic structure changes and the origin of the enhanced optical properties in N-doped anatase TiO<sub>2</sub>—A theoretical revisit. *J. Appl. Phys.* **2014**, *116*, 093709. [[CrossRef](#)]
57. Hu, S.; Wang, A.; Li, X.; Löwe, H. Hydrothermal synthesis of well-dispersed ultrafine N-doped TiO<sub>2</sub> nanoparticles with enhanced photocatalytic activity under visible light. *J. Phys. Chem. Solids* **2010**, *71*, 156–162. [[CrossRef](#)]
58. Rizzo, L.; Meric, S.; Kassinos, D.; Guida, M.; Russo, F.; Belgiorno, V. Degradation of diclofenac by TiO<sub>2</sub> photocatalysis: UV absorbance kinetics and process evaluation through a set of toxicity bioassays. *Water Res.* **2009**, *43*, 979–988. [[CrossRef](#)]